

## Crystalline finite-size topology

Michał J. Pacholski and Ashley M. Cook 

*Max Planck Institute for Chemical Physics of Solids, Nöthnitzer Strasse 40, 01187 Dresden, Germany*  
*and Max Planck Institute for the Physics of Complex Systems, Nöthnitzer Strasse 38, 01187 Dresden, Germany*



(Received 29 December 2023; revised 2 June 2024; accepted 4 June 2024; published 12 June 2024)

Topological phases stabilized by crystalline point group symmetry protection are a large class of symmetry-protected topological phases subjected to considerable experimental scrutiny. Here, we show that the canonical three-dimensional (3D) crystalline topological insulator protected by time-reversal symmetry  $\mathcal{T}$  and fourfold rotation symmetry  $C_4$  individually or the product symmetry  $C_4\mathcal{T}$ , generically realizes finite-size crystalline topological phases in thin film geometry [a quasi-(3-1)-dimensional, or q(3-1)D, geometry]: response signatures of the 3D bulk topology coexist with topologically protected, quasi-(3-2)D, and quasi-(3-3)D boundary modes within the energy gap resulting from strong hybridization of the Dirac cone surface states of the underlying 3D crystalline topological phase. Importantly, we find qualitative distinctions between these gapless boundary modes and those of strictly 2D crystalline topological states with the same symmetry protection and develop a low-energy, analytical theory of the finite-size topological magnetoelectric response.

DOI: [10.1103/PhysRevB.109.235125](https://doi.org/10.1103/PhysRevB.109.235125)

Crystalline topological phases, or those protected in whole or in part by crystalline point group symmetries, have been a very active front in efforts to identify and classify topologically nontrivial phases of matter. The large number of crystalline point group symmetries protect many distinctive topological insulator and semimetal states [1–22], building extensively on the foundational work of the tenfold way classification scheme [23,24]. Recent work reveals, however, that these canonical  $D$ -dimensional states, such as the Chern insulator [25], or the strong topological insulator [26], can remain relevant even when the system is only thermodynamically large in  $\delta < D$  directions [27,28]: for example, taking  $\delta = 1$ , even if  $(D-1)$ -dimensional gapless boundary modes associated with a  $D$ -dimensional bulk topological invariant are lost due to strong hybridization,  $D$ -dimensional topological response signatures can coexist with quasi- $(D-2)$ -dimensional [q( $D-2$ )D] gapless boundary modes in the form of finite-size topological phases (FSTs) [27]. A degree of freedom taking  $N$  different values, corresponding to an  $N$ -fold degree of freedom, with  $1 < N < 10$ , can then potentially serve as a synthetic dimension, greatly enriching physics of band topology.

Finite-size topological phases are one of three recently identified sets of phases of matter consistent with generalization of the framework of the quantum Hall effect—and associated classification schemes—to that of the quantum skyrmion Hall effect (QSkHE) [29], which requires incorporating compactified  $p$ -brane charged excitations—or fuzzy (pseudo)psin skyrmions—into classification. How to suitably generalize classification methods, even one of the most robust,

such as K theory [30], to capture the QSKHE is currently unknown. This motivates introduction of canonical examples of FST phases first as part of eventually developing systematic classification tools. In this work, we demonstrate FSTs are also stabilized by crystalline point group symmetries, studying the FST counterpart of the canonical crystalline topological phase [1]. The present work therefore indicates the vast family of crystalline topological phases may yield FSTs and provides a blueprint for their study.

We focus on the canonical Hamiltonian for the first formally identified crystalline topological phase [1], a 3D topological insulator protected by fourfold rotational symmetry and time-reversal symmetry. That is, we confirm that a system realizing the canonical crystalline topological state in the 3D bulk, but which is thermodynamically large in only two spatial dimensions, realizes quasi-(3-3)D gapless boundary corner states or quasi-(3-2)D gapless boundary edge states when 2D gapless boundary modes of the 3D phase strongly hybridize, while still possessing the topological response signature of the 3D bulk invariant. The system geometries and procedures for confirming these two defining properties of finite-size topological phases are shown schematically in Fig. 1. Our work therefore lays the foundation for far broader study of topological phases protected in whole or in part by crystalline point group symmetries, with the foundational results presented here particularly important in understanding of van der Waals thin films and heterostructures [31–39] identified as hosting 2D or quasi-1D topological states, which may actually be partially identified finite-size topological phases instead descending from underlying higher-dimensional bulk topology.

### I. HAMILTONIAN

We consider a Hamiltonian previously introduced by Fu [1] realizing the crystalline topological insulator phase. The

*Published by the American Physical Society under the terms of the Creative Commons Attribution 4.0 International license. Further distribution of this work must maintain attribution to the author(s) and the published article's title, journal citation, and DOI. Open access publication funded by Max Planck Society.*

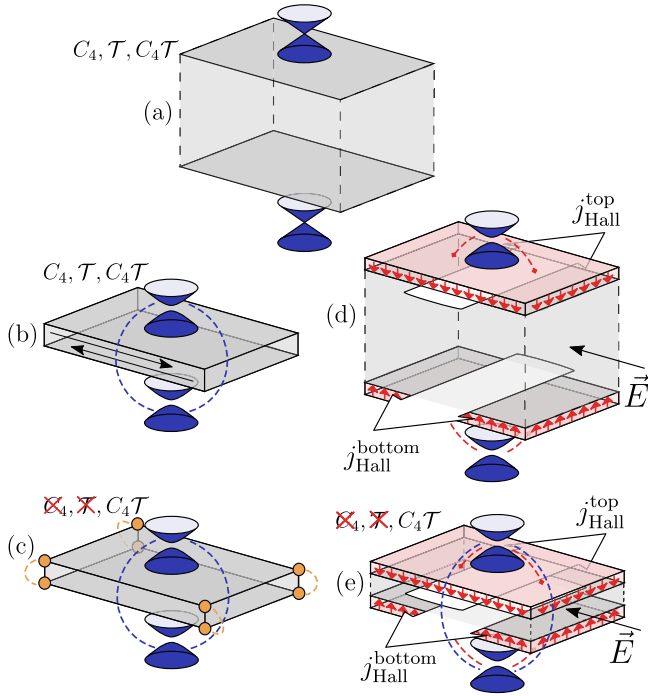


FIG. 1. Demonstrating crystalline finite-size topology. (a) 3D crystalline topological insulator with Dirac cone surface states. Panels (b) and (c) depict bulk-boundary correspondence of system in thin-film geometry either with time-reversal symmetry (TRS) and fourfold rotation symmetry ( $C_4$ ) individually present or without, respectively, corresponding to a finite-size topological phase. (d) 3D system with magnetic surface perturbations to probe quantized surface Hall conductivity associated with the 3D topological state; (e) a system in thin film geometry realizing bulk-boundary correspondences of (b) and (c), with magnetic surface perturbations to confirm topological magnetoelectric response of the finite-size topological phase.

Bloch Hamiltonian is taken to be

$$H(\mathbf{k}) = \left( M + t \sum_{i \in \{x,y,z\}} \cos k_i \right) \tau_z \sigma_0 + \Delta_1 \tau_x \sigma \cdot \sin \mathbf{k} + (\cos k_x - \cos k_y) (\Delta_2 \tau_y \sigma_0 + \Delta_3 \tau_0 \sigma_z). \quad (1)$$

At  $\Delta_2 = \Delta_3 = 0$ , the Hamiltonian respects both time-reversal symmetry  $\mathcal{T} = \sigma_y \mathcal{K}$  and fourfold rotation symmetry

$$C_4 = e^{i(\sigma_z/2 + xk_y - yk_x)\pi/2}, \quad (2)$$

which acts as

$$\begin{aligned} C_4^\dagger(k_x, k_y, k_z)C_4 &= (k_y, -k_x, k_z), \\ C_4^\dagger(\sigma_x, \sigma_y, \sigma_z)C_4 &= (\sigma_y, -\sigma_x, \sigma_z). \end{aligned} \quad (3)$$

The terms proportional to  $\Delta_2, \Delta_3$  are the simplest such terms (i.e., containing only nearest-neighbor hoppings) that break both  $\mathcal{T}$  and  $C_4$  symmetries, while preserving their product  $C_4\mathcal{T}$ .

## II. PHASE DIAGRAM

We are interested in characterizing the phase diagram of this model, in particular in a finite-thickness slab geometry,

and its properties that generalize to arbitrary systems in the class of  $C_4\mathcal{T}$ -symmetric crystalline topological insulators. To do so, we first briefly review standard characterization for the system thermodynamically large in three space dimensions. In three dimensions, the model is characterized by a  $\mathbb{Z}_2$  invariant, which distinguishes phases with and without gapless Dirac cones at the  $C_4\mathcal{T}$ -invariant surfaces (i.e.,  $z = \text{const}$ ).

We can demonstrate this bulk-boundary correspondence by calculating the surface states of our toy model. We know that the Dirac point will be located at a  $C_4\mathcal{T}$ -invariant surface momentum  $(k_x, k_y) = q \in \{(0, 0), (\pi, \pi)\}$  and, due to the presence of an additional artificial particle-hole symmetry  $\mathcal{C} = \tau_y \sigma_y \mathcal{K}$ , the surface-gap closing will occur at energy  $E = 0$  and the zero mode will be an eigenstate of chiral symmetry operator  $\mathcal{T}\mathcal{C} = \tau_y$ :  $\tau_y \psi = \chi \psi$ ,  $\chi = \pm 1$ . The gap closing condition then reads

$$(m_q + t \cos k_z + i\chi \Delta_1 \sigma_z \sin k_z) \psi = 0, \quad (4)$$

where  $m_{0,0} = M + 2t$  and  $m_{\pi,\pi} = M - 2t$ . Solving for  $k_z$ , we find

$$e^{ik_z} = \frac{-m_q \pm \sqrt{m_q^2 + \Delta_1^2 - t^2}}{t + s\chi \Delta_1}, \quad (5)$$

with  $s = \pm 1$  and  $\sigma_z \psi = s\psi$ .

For a state with given  $\chi, s$  to be decaying at  $z \rightarrow \infty$ , there must be two solutions for  $k_z$ , satisfying  $|e^{ik_z}| < 1$ . This is true if and only if  $\chi s = \text{sgn}(\Delta_1/t)$  and  $|m_q| < |t|$ .

If cones are present at both  $q = (0, 0)$  and  $q = (\pi, \pi)$  simultaneously, they are no longer protected, which results in a trivial phase. This leads to a nontrivial bulk-topological phase for  $-3|t| < M < -|t|$  and  $2|t| < M < 3|t|$ .

## III. QUASI-(3-1)D THIN-FILM GEOMETRY

Now, we will turn our attention to a slab of thickness  $L$  finite in the  $z$  direction. Here, we discuss the example of  $L = 4$  in detail and include information on other values of  $L$  in the Supplemental Material (SM) [40]. In particular, we demonstrate the effect of  $L$  odd or even on the topological phase diagram. In a topological region of the 3D bulk phase diagram, the overlap between the surface states on the two surfaces will produce a surface hybridization gap, which may oscillate with the slab thickness and the parameters of the model.

We can capture this phenomenology with a low-energy model of the surface states. Assuming that the slab spans  $0 < z \leq L$ , we know that the surface states at  $z = 0$  will have  $\chi s = \text{sgn}(\Delta_1/t)$ , whereas those at  $z = L$  will have  $\chi s = -\text{sgn}(\Delta_1/t)$ . For a surface momentum close to the Dirac point  $(k_x, k_y) = q + \delta q$ , we can project the Hamiltonian onto the subspace spanned by the surface states. Taking for concreteness  $t = 1, \Delta_1 > 0$ , we then get the low energy effective Hamiltonian (additional details of derivation provided in the SM [40])

$$\begin{aligned} h &= \Delta_1 v_0 (\sigma_x \delta q_x + \sigma_y \delta q_y) + v_y \sigma_z \delta \\ &+ s_q (\delta q_x^2 - \delta q_y^2) (\Delta_2 v_z \sigma_z + \Delta_3 v_0 \sigma_z), \end{aligned} \quad (6)$$

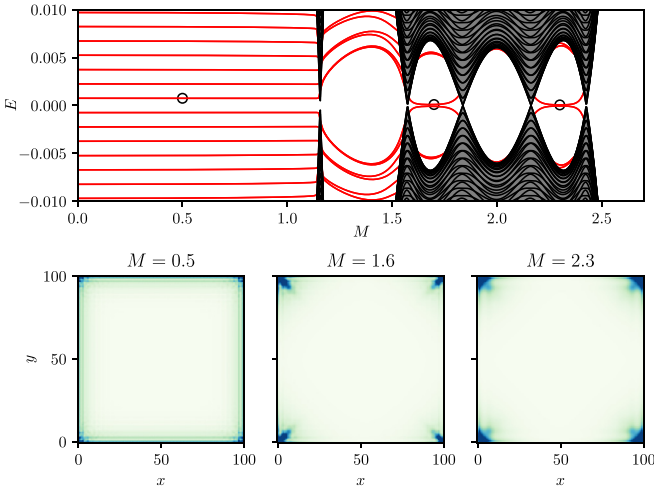


FIG. 2. Bulk-boundary correspondence of finite-size crystalline topological phase: (a) energy spectrum vs mass term  $M$  of a system in thin film geometry with OBC in the  $\hat{z}$  direction (black) and OBC in each spatial direction (red). Panels (b), (c), and (d) depict charge density distribution vs  $x$  and  $y$  for states highlighted by black circles in (a) corresponding to  $M = 0.5, 1.6,$  and  $2.3,$  respectively. The values of the remaining parameters used were  $t = -1, \Delta_1 = 0.6, \Delta_2 = 0.37,$  and  $\Delta_3 = 0.4.$

where  $v_\alpha$  is a set of Pauli matrices acting in the surface-index degree of freedom,  $\delta$  is the hybridization gap, and  $s_{0,0} = -1, s_{\pi,\pi} = 1.$

Let us now consider a slab finite in  $x, y$  directions (with size  $W \gg L$ ). The vacuum can be modeled by taking  $\delta \rightarrow \infty.$  If time-reversal symmetry is preserved ( $\Delta_2 = \Delta_3 = 0$ ) and  $\delta < 0$  in the interior of the slab, we expect the edge states propagating along the edges. We shall find them analytically. For an edge along  $\mathbf{n}_\parallel = (\cos \alpha, \sin \alpha),$  with vacuum at  $\mathbf{r} \cdot \mathbf{n}_\perp < 0, \mathbf{n}_\perp = \mathbf{n}_\parallel \times \hat{\mathbf{z}} = (\sin \alpha, -\cos \alpha)$  is a unit vector pointing towards the bulk of the slab; the boundary condition is  $v_y(\mathbf{n}_\parallel \cdot \boldsymbol{\sigma})\psi = -\psi.$  The edge-state solutions are then

$$\psi_{\pm} \propto e^{-(\delta/\Delta_1)\mathbf{r} \cdot \mathbf{n}_\perp} e^{i\delta q_\parallel \mathbf{r} \cdot \mathbf{n}_\parallel} \begin{pmatrix} 1 \\ \pm i \end{pmatrix}_v \begin{pmatrix} 1 \\ \mp e^{i\alpha} \end{pmatrix}_\sigma, \quad (7)$$

with corresponding energies

$$E_{\pm}(q_\parallel) = \mp \Delta_1 \delta q_\parallel, \quad (8)$$

where  $\delta q_\parallel$  is the momentum along the edge. Projecting the low-energy slab Hamiltonian onto the edge-state Hilbert space—this time allowing for nonzero  $\Delta_2, \Delta_3$ —we get a low-energy edge Hamiltonian

$$h' = -\Delta_1 q_\parallel v_y + s_q \frac{\Delta_2 \delta^2}{\Delta_1^2} \cos(2\alpha) v_z. \quad (9)$$

The mass term proportional to  $v_z$  changes sign at the points where edge orientation is  $\alpha \in \{\pi/4, 3\pi/4, 5\pi/4, 7\pi/4\},$  at which points there will be corner zero-energy bound states. These corner states will be eigenstates of  $v_x,$  so their charge distribution will be equally split between the top and the bottom surface.

We support the above analytical calculations with numerical results for the quasi-(3-1)D slab shown in Fig. 2,

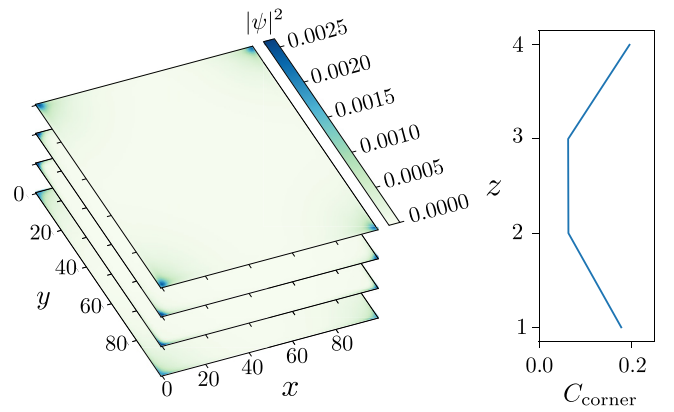


FIG. 3. Left panel: probability density distribution over real-space for the corner mode shown in Fig. 2 at  $M = 1.6,$  with four unit cells in the stacking ( $z$ ) direction. Right panel: charge density per corner vs layer index in the stacking ( $z$ ) direction.

with open-boundary conditions in first the  $z$  direction (black) and then also in the  $x$  and  $y$  directions (red). We characterize the quasi-(3-1)D bulk topology with the topological invariant  $\nu$  [41]

$$\nu = \frac{1}{\pi} \left[ \int_{\text{IBZ}} \text{Tr} \mathcal{F} dk^2 + 2i \log \det \mathcal{W}_{\Gamma \rightarrow M} \right] \text{ mod } 4, \quad (10)$$

defined over the irreducible Brillouin zone (IBZ), where  $\mathcal{F}$  is the non-Abelian Berry curvature and  $\det \mathcal{W}_{\mathcal{C}}$  is the dressed Wilson line determinant.

In the case when  $\Delta_2 = 0,$  this invariant can be calculated explicitly for the effective low energy Hamiltonian [40]:

$$\nu = 1 - \text{sgn}(\delta_{0,0}\delta_{\pi,\pi}) - \text{sgn}(2\Delta_3 + \delta_{0,\pi}) + \text{sgn}(2\Delta_3 - \delta_{0,\pi}) \text{ mod } 4. \quad (11)$$

When  $\mathcal{T}$  and  $C_4$  are present ( $\Delta_2 = \Delta_3 = 0$ ),  $\nu$  is  $\mathbb{Z}_2$  classified and  $\mathbb{Z}_4$  when these symmetries are broken while preserving  $C_4\mathcal{T}.$  As shown in Fig. 2, nontrivial  $\nu$  corresponds to quasi-(3-2)D gapless edge states ( $\nu = 1, 3$ ) or quasi-(3-3)D corner modes ( $\nu = 2$ ) for this geometry.

It is important to explicitly distinguish between corner states of a strictly 2D topological phase and the corner states of the finite-size topological phase presented here. The probability density distribution of boundary states in the finite-size topological phase are noticeably  $z$  dependent as shown in Fig. 3, with charge density concentrated at the corners of the top and bottom layers specifically, rather than evenly distributed along the hinges. This bulk-boundary correspondence distinguishes the finite-size topological phase from a strictly 2D crystalline topological state. While uneven distribution of corner charge in the stacking direction for a strictly 2D crystalline topological state is possible, in principle, the topological state does not protect it. In the case of the quasi-(3-1)D crystalline FST phase, it is protected, as the corner states originate specifically from the gapped surface states of the top and bottom surfaces.

#### IV. TOPOLOGICAL RESPONSE SIGNATURES OF FINITE-SIZE TOPOLOGY

We may also examine the topological response of the system normally associated with a 3D bulk, the topological magnetoelectric polarizability [42], for the system in the quasi-(3-1)D geometry, to further investigate the nature of the topological nontrivial state. To do so, we introduce magnetic perturbations at the top and bottom surfaces of the quasi-(3-1)D system as illustrated in Fig. 1(e).

We model the magnetic perturbation by adding a term  $\tilde{\kappa} v_z \sigma_z$  to the effective surface Hamiltonian (6):

$$h = \Delta_1 v_0 (\sigma_x \delta q_x + \sigma_y \delta q_y) + v_y \sigma_z \delta + \tilde{\kappa} v_z \sigma_z. \quad (12)$$

The Hall conductivity of the top/bottom surfaces is given by the formula [42]

$$C_{\pm} = \frac{i}{2\pi} \int dk \text{Tr}[P \epsilon_{ij} (\partial_i P) v_{\pm} (\partial_j P)], \quad (13)$$

where  $P$  is the ground-state projector and  $v_{\pm} = \frac{1}{2}(v_0 \pm v_z)$  is the projector onto the top/bottom surface. We can find the spectrum of the Hamiltonian by squaring it,

$$H^2 = \epsilon^2, \quad \epsilon = \sqrt{v^2 k_x^2 + v^2 k_y^2 + \delta^2 + \tilde{\kappa}^2}, \quad (14)$$

and thus the ground-state projector is simply

$$P = \frac{\epsilon - H}{2\epsilon}. \quad (15)$$

We then get

$$\text{Tr}[P \epsilon_{ij} (\partial_i P) v_{\pm} (\partial_j P)] = \mp \frac{i\tilde{\kappa}}{2\epsilon^3}, \quad (16)$$

which yields

$$C_{\pm} = \pm \frac{\tilde{\kappa}}{2\sqrt{\delta^2 + \tilde{\kappa}^2}}. \quad (17)$$

In the case when the magnetization-induced gap dominates over the hybridization gap, this tends to the expected value  $1/2$ . These results may provide additional understanding of past work on the magnetoelectric polarizability of axion insulators in thin film systems, where deviations from  $1/2$  are also observed as part of the topological response signature [39].

Numerical results on the response signatures associated with the topological magnetoelectric polarizability are shown in Fig. 4. Surface Hall conductance for the top layer is shown over the same interval in mass parameter  $M$  as in Fig. 2 as a function of magnetization strength  $\kappa$ . We see that, with increasing  $\kappa$ , the surface Hall conductance increasingly approaches a saturation value of  $0.5$  in units of  $e^2/h$ , the value associated with nontrivial magnetoelectric polarizability [42], over the region of the underlying bulk 3D topological state. For very small  $\kappa$ , finite surface Hall conductance first nucleates about the transition points between topological bubbles corresponding to different finite-size topological states, competing with the hybridization gap. This demonstrates that, even if the gapless surface states associated with the 3D bulk topological phase strongly hybridize and are lost, in this sense, due to finite-size effects, the 3D bulk topological invariant remains very relevant in characterizing the topological state and the quasi-(3-1)D system is not adequately characterized

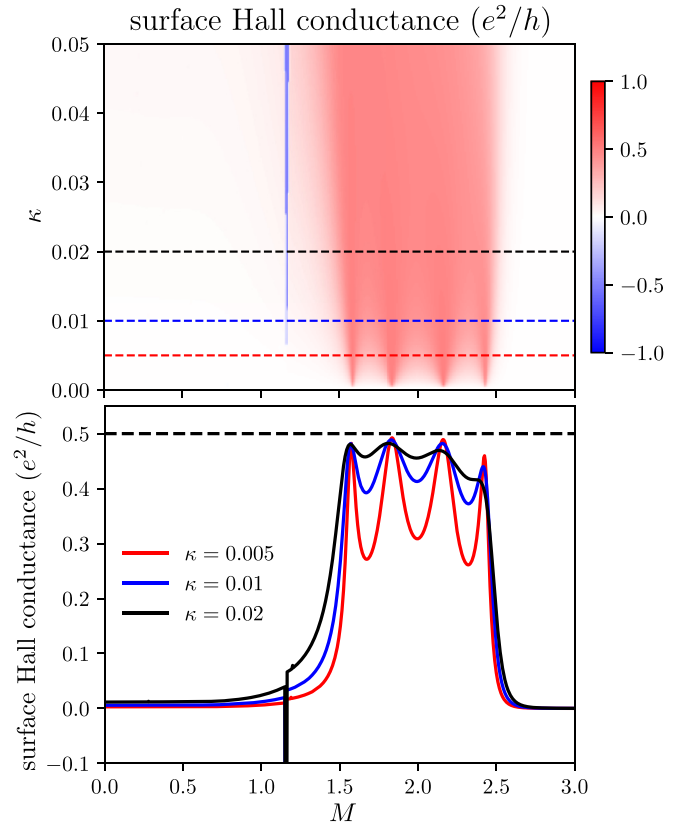


FIG. 4. Topological magnetoelectric response of a finite-size crystalline topological phase: (a) surface Hall conductance vs mass term  $M$  and surface magnetization strength  $\kappa$ . Panel (b) depicts cuts through (a) for different fixed magnetization strengths  $\kappa$ .

by topological invariants of strictly 2D, 1D, and/or 0D bulk. This may help explain recent experiments in thin-film systems investigating states with nontrivial magnetoelectric polarizability [39,43–45]. For this purpose, we show the dependence of the topological magnetoelectric response on system size  $L$  in the Supplemental Material [40].

#### V. DISCUSSION AND CONCLUSION

We introduce crystalline finite-size topological phases of matter in this work. We examine the Hamiltonian of the canonical crystalline topological insulator state protected by fourfold rotational symmetry and time-reversal symmetry or invariance of the system under the product operation of fourfold rotation and time reversal [1]. For open boundary conditions in the  $z$  direction, with corresponding system size in this direction,  $L$ , on the scale of a few unit cells (e.g.,  $L < 10$ ), we find the gapless surface states occurring for thermodynamically large  $L$  generically strongly hybridize to open a gap, with gapless regions reduced to gapped, fine-tuned *transition* points between topologically distinct gapped regions of the phase diagram. These gapped regions may be topologically characterized to determine an additional bulk-boundary correspondence distinct from that of strictly 2D topological states, with nontrivial invariant indicating gapless edge or corner states concentrated at the top and bottom surfaces upon opening boundary conditions in

the  $x$  and  $y$  directions such that the protecting symmetries of the bulk state are preserved at the boundary. As required for a finite-size topological phase, however, we also confirm the layer-dependent Hall conductance signature of nontrivial magnetoelectric polarizability persists for  $L < 10$  even when the surface states of the underlying 3D state are absent due to strong hybridization.

Our work therefore serves as a foundation in studying finite-size topology of the large class of topological states protected in whole or in part by crystalline point group symmetries and studied heavily in experiments. Our work may

furthermore provide understanding of topological response signatures of intrinsically three-dimensional topological states previously-observed in thin film systems [39,43–45].

#### ACKNOWLEDGMENTS

This research was supported in part by the National Science Foundation under Grants No. NSF PHY-1748958 and No. PHY-2309135 and undertaken in part at Aspen Center for Physics, which is supported by National Science Foundation Grant No. PHY-2210452.

- 
- [1] L. Fu, Topological crystalline insulators, *Phys. Rev. Lett.* **106**, 106802 (2011).
  - [2] W. A. Benalcazar, B. A. Bernevig, and T. L. Hughes, Quantized electric multipole insulators, *Science* **357**, 61 (2017).
  - [3] Y. Tanaka, Z. Ren, T. Sato, K. Nakayama, S. Souma, T. Takahashi, K. Segawa, and Y. Ando, Experimental realization of a topological crystalline insulator in SnTe, *Nat. Phys.* **8**, 800 (2012).
  - [4] H. Weng, J. Zhao, Z. Wang, Z. Fang, and X. Dai, Topological crystalline kondo insulator in mixed valence ytterbium borides, *Phys. Rev. Lett.* **112**, 016403 (2014).
  - [5] Y. Ando and L. Fu, Topological crystalline insulators and topological superconductors: From concepts to materials, *Annu. Rev. Condens. Matter Phys.* **6**, 361 (2015).
  - [6] B. J. Wieder, B. Bradlyn, Z. Wang, J. Cano, Y. Kim, H.-S. D. Kim, A. M. Rappe, C. L. Kane, and B. A. Bernevig, Wallpaper fermions and the nonsymmorphic Dirac insulator, *Science* **361**, 246 (2018).
  - [7] A. M. Turner, Y. Zhang, R. S. K. Mong, and A. Vishwanath, Quantized response and topology of magnetic insulators with inversion symmetry, *Phys. Rev. B* **85**, 165120 (2012).
  - [8] T. L. Hughes, E. Prodan, and B. A. Bernevig, Inversion-symmetric topological insulators, *Phys. Rev. B* **83**, 245132 (2011).
  - [9] C. Fang, M. J. Gilbert, and B. A. Bernevig, Bulk topological invariants in noninteracting point group symmetric insulators, *Phys. Rev. B* **86**, 115112 (2012).
  - [10] A. M. Turner, Y. Zhang, and A. Vishwanath, Entanglement and inversion symmetry in topological insulators, *Phys. Rev. B* **82**, 241102(R) (2010).
  - [11] K. Shiozaki, M. Sato, and K. Gomi,  $Z_2$  topology in nonsymmorphic crystalline insulators: Möbius twist in surface states, *Phys. Rev. B* **91**, 155120 (2015).
  - [12] K. Shiozaki, M. Sato, and K. Gomi, Topology of nonsymmorphic crystalline insulators and superconductors, *Phys. Rev. B* **93**, 195413 (2016).
  - [13] K. Shiozaki, M. Sato, and K. Gomi, Topological crystalline materials: General formulation, module structure, and wallpaper groups, *Phys. Rev. B* **95**, 235425 (2017).
  - [14] M. I. Aroyo, A. Kirov, C. Capillas, J. M. Perez-Mato, and H. Wondratschek, Bilbao crystallographic server. II. Representations of crystallographic point groups and space groups, *Acta Cryst. Sect. A* **62**, 115 (2006).
  - [15] R.-J. Slager, A. Mesaros, V. Jurii, and J. Zaanen, The space group classification of topological band-insulators, *Nat. Phys.* **9**, 98 (2013).
  - [16] J. Kruthoff, J. de Boer, J. van Wezel, C. L. Kane, and R.-J. Slager, Topological classification of crystalline insulators through band structure combinatorics, *Phys. Rev. X* **7**, 041069 (2017).
  - [17] H. C. Po, H. Watanabe, M. P. Zaletel, and A. Vishwanath, Filling-enforced quantum band insulators in spin-orbit coupled crystals, *Sci. Adv.* **2**, e1501782 (2016).
  - [18] A. Alexandradinata and B. A. Bernevig, Berry-phase description of topological crystalline insulators, *Phys. Rev. B* **93**, 205104 (2016).
  - [19] H. Watanabe, H. C. Po, A. Vishwanath, and M. Zaletel, Filling constraints for spin-orbit coupled insulators in symmorphic and nonsymmorphic crystals, *Proc. Natl. Acad. Sci. USA* **112**, 14551 (2015).
  - [20] H. Watanabe, H. C. Po, M. P. Zaletel, and A. Vishwanath, Filling-enforced gaplessness in band structures of the 230 space groups, *Phys. Rev. Lett.* **117**, 096404 (2016).
  - [21] B. Bradlyn, L. Elcoro, J. Cano, M. G. Vergniory, Z. Wang, C. Felser, M. I. Aroyo, and B. A. Bernevig, Topological quantum chemistry, *Nature (London)* **547**, 298 (2017).
  - [22] D. Varjas, F. de Juan, and Y.-M. Lu, Space group constraints on weak indices in topological insulators, *Phys. Rev. B* **96**, 035115 (2017).
  - [23] S. Ryu, A. P. Schnyder, A. Furusaki, and A. W. W. Ludwig, Topological insulators and superconductors: Tenfold way and dimensional hierarchy, *New J. Phys.* **12**, 065010 (2010).
  - [24] A. P. Schnyder, S. Ryu, A. Furusaki, and A. W. W. Ludwig, Classification of topological insulators and superconductors in three spatial dimensions, *Phys. Rev. B* **78**, 195125 (2008).
  - [25] F. D. M. Haldane, Model for a quantum Hall effect without Landau levels: Condensed-matter realization of the “parity anomaly”, *Phys. Rev. Lett.* **61**, 2015 (1988).
  - [26] J. E. Moore and L. Balents, Topological invariants of time-reversal-invariant band structures, *Phys. Rev. B* **75**, 121306(R) (2007).
  - [27] A. M. Cook and A. E. B. Nielsen, Finite-size topology, *Phys. Rev. B* **108**, 045144 (2023).
  - [28] R. Flores-Calderon, R. Moessner, and A. M. Cook, Time-reversal invariant finite-size topology, *Phys. Rev. B* **108**, 125410 (2023).

- [29] A. M. Cook, Quantum skyrmion Hall effect, *Phys. Rev. B* **109**, 155123 (2024).
- [30] A. Kitaev, Periodic table for topological insulators and superconductors, in *AIP Conf. Proc. No. 1134* (AIP, Melville, NY, 2009), p. 22.
- [31] A. K. Geim and I. V. Grigorieva, Van der Waals heterostructures, *Nature (London)* **499**, 419 (2013).
- [32] C. Hu, K. N. Gordon, P. Liu, J. Liu, X. Zhou, P. Hao, D. Narayan, E. Emmanouilidou, H. Sun, Y. Liu, H. Brawer, A. P. Ramirez, L. Ding, H. Cao, Q. Liu, D. Dessau, and N. Ni, A van der Waals antiferromagnetic topological insulator with weak interlayer magnetic coupling, *Nat. Commun.* **11**, 97 (2020).
- [33] S. Kong Chong, K. Bum Han, A. Nagaoka, R. Tsuchikawa, R. Liu, H. Liu, Z. Vally Vardeny, D. A. Pesin, C. Lee, T. D. Sparks, and V. V. Deshpande, Topological insulator-based van der Waals heterostructures for effective control of massless and massive Dirac fermions, *Nano Lett.* **18**, 8047 (2018).
- [34] L. Kou, S.-Chun Wu, C. Felser, T. Frauenheim, C. Chen, and B. Yan, Robust 2d topological insulators in van der Waals heterostructures, *ACS Nano* **8**, 10448 (2014).
- [35] S. Husain, R. Gupta, A. Kumar, P. Kumar, N. Behera, R. Brucas, S. Chaudhary, and P. Svedlindh, Emergence of spin orbit torques in 2d transition metal dichalcogenides: A status update, *Appl. Phys. Rev.* **7**, 041312 (2020).
- [36] D. Varsano, M. Palummo, E. Molinari, and M. Rontani, A monolayer transition-metal dichalcogenide as a topological excitonic insulator, *Nat. Nanotechnol.* **15**, 367 (2020).
- [37] P. Song, C. Hsu, M. Zhao, X. Zhao, T.-Rong Chang, J. Teng, H. Lin, and K. Ping Loh, Few-layer 1t' MoTe<sub>2</sub> as gapless semimetal with thickness dependent carrier transport, *2D Mater.* **5**, 031010 (2018).
- [38] X. Qian, J. Liu, L. Fu, and J. Li, Quantum spin Hall effect in two-dimensional transition metal dichalcogenides, *Science* **346**, 1344 (2014).
- [39] M. Kawamura, M. Mogi, R. Yoshimi, T. Morimoto, K. S. Takahashi, A. Tsukazaki, N. Nagaosa, M. Kawasaki, and Y. Tokura, Laughlin charge pumping in a quantum anomalous Hall insulator, *Nat. Phys.* **19**, 333 (2023).
- [40] See Supplemental Material at <http://link.aps.org/supplemental/10.1103/PhysRevB.109.235125> for derivation of the low-energy effective Hamiltonian and details of topological invariants.
- [41] I. Araya Day, A. Varentcova, D. Varjas, and A. R. Akhmerov, Pfaffian invariant identifies magnetic obstructed atomic insulators, *SciPost Phys.* **15**, 114 (2023).
- [42] A. M. Essin, J. E. Moore, and D. Vanderbilt, Magnetoelectric polarizability and axion electrodynamics in crystalline insulators, *Phys. Rev. Lett.* **102**, 146805 (2009).
- [43] C. Liu, Y. Wang, H. Li, Y. Wu, Y. Li, J. Li, K. He, Y. Xu, J. Zhang, and Y. Wang, Robust axion insulator and Chern insulator phases in a two-dimensional antiferromagnetic topological insulator, *Nat. Mater.* **19**, 522 (2020).
- [44] Y. Li, C. Liu, Y. Wang, Z. Lian, S. Li, H. Li, Y. Wu, H.-Z. Lu, J. Zhang, and Y. Wang, Giant nonlocal edge conduction in the axion insulator state of MnBi<sub>2</sub>Te<sub>4</sub>, *Sci. Bull.* **68**, 1252 (2023).
- [45] C. Liu, Y. Wang, M. Yang, J. Mao, H. Li, Y. Li, J. Li, H. Zhu, J. Wang, L. Li, Y. Wu, Y. Xu, J. Zhang, and Y. Wang, Magnetic-field-induced robust zero Hall plateau state in MnBi<sub>2</sub>Te<sub>4</sub> Chern insulator, *Nat. Commun.* **12**, 4647 (2021).